(1957).
[3]H. S. Köhler, Nucl. Phys. 88, 529 (1966).
[4]H. P. Kelly, Phys. Rev. 131, 684 (1963).
[5]H. P. Kelly, Advan. Chem. Phys. 14, 129 (1969).
[6]H. J. Silverstone and M. L. Yin, J. Chem. Phys. 49, 2076 (1968).
[7]S. Huzinaga and C. Arnau, Phys. Rev. A 1, 2285 (1970).
[8]H. P. Kelly, Phys. Rev. 144, 39 (1966).
[9]J. H. Miller and H. P. Kelly, Phys. Rev. A (to be published).
[10]P. S. Bagus, Phys. Rev. 139, A619 (1965).
[11]C. Froese, Can. J. Phys. 41, 1895 (1963), and subsequent revisions.
[12]See especially the discussion on p. 144 of Ref. 5.
[13]H. P. Kelly, Phys. Rev. 173, 142 (1968).
[14]E. R. Davidson and T. L. Barr, Phys. Rev. A 1, 644 (1970).
[15]J. W. Viers, F. E. Harris, and H. F. Schaefer, III, Phys. Rev. A 1, 14 (1970).
[16]E. Clementi, J. Chem. Phys. 39, 175 (1963).
[17]*Atomic Energy Levels*, edited by C. E. Moore, National Bureau of Standards Circular No. 467 (U.S. GPO, Washington, D.C., 1949).
[18]E. J. McGuire, Phys. Rev. 185, 1 (1969).
[19]H. P. Kelly, Phys. Rev. 136, B896 (1964).
[20]W. F. Frey, R. E. Johnston, and J. I. Hopkins, Phys. Rev. 113, 1057 (1959).
[21]J. Heinz, Z. Physik 143, 153 (1955).

PHYSICAL REVIEW A VOLUME 3, NUMBER 5 MAY 1971

Measurement of Lifetime and g Factors by Level Crossing and Optical Double Resonance in the OH and OD Free Radicals

Robert L. deZafra, Alan Marshall, * and Harold Metcalf
State University of New York, Stony Brook, New York 11790
(Received 1 October 1970; revised manuscript received 22 January 1971)

The zero-field level crossing and optical double-resonance techniques have been used to measure the lifetimes and g factors of several rotational substates in the $A^2\Sigma^+$ excited state of the OH and OD free radicals. Optical excitation was provided by a molecular lamp and individual emission transitions were observed through a monochromator in the beam of resonantly scattered light. The measured g factors are in agreement with the results expected from pure case b coupling for this state. The measured lifetimes are 660 ± 22 and 598 ± 20 nsec for OH and OD, respectively; the mean value 629 ± 22 nsec is suggested. The optical double-resonance experiments allow a tentative lower limit to be placed on the excited-state hyperfine interaction.

I. INTRODUCTION

Over the past decade, the Hanle effect (also called the zero-field level-crossing technique)[1] has been used to obtain precision values for lifetimes, g factors, and hyperfine splittings in the electronic excited states of a large variety of atoms. More recently, attention has turned to the extension of this technique, along with the older optical double-resonance (ODR) technique, to obtain molecular parameters and lifetimes of excited molecular states.[2-5] This paper discusses these techniques as we have applied them to a study of the $A^2\Sigma^+$ state of the OH and OD free radicals. Some of the work included here has been previously reported.[3]

From the theoretical point of view, the extension of level crossing to molecular systems is quite straightforward.[4] However, molecules can present rather formidable experimental problems, most of which arise from the rotational and vibrational structure of the electronic states. In particular, because of the rotational structure, single electronic transitions in a typical diatomic molecule give rise to the familiar bands of closely spaced lines, separated by no more than a few tenths of an angstrom, which connect different rotational sublevels between various electronic states. Since the detailed nature of a level-crossing signal depends strongly on the total angular momentum of the initial, excited, and final states, it is necessary to resolve single lines in the band structure in order to fully interpret an experiment. For example, in order to measure the dependence of properties such as g factors on the rotational quantum number of the excited state, it is clearly desirable to isolate single rotational-vibrational transitions.

German and Zare,[5] in experiments similar to ours, surmounted this problem by taking advantage of the fortuitous overlap of an atomic line with one rotational transition in the $A^2\Sigma$-$X^2\Pi$ band of OH. Using the atomic line to excite the molecules, they were able to measure the g factor and lifetime of the $K' = 2$, $J' = \frac{3}{2}$ rotational level of the OH molecule, but this method does not permit a systematic study over rotational levels. In a different approach Isler and Wells[6] used the entire 1-0 band in a CO discharge lamp to provide resonance excitation for a zero-field level-crossing experiment in CO. They attempted to take into account the contributions of the numerous different rotational levels theoretical-

ly. This method has promise for the measurement of lifetimes in states where no serious perturbations are present, but may not be satisfactory in cases where the lifetime or other parameters to be measured show any marked variation within a rotational band.

Our choice of the OH molecule as a candidate for initial testing of level-crossing techniques in molecules was motivated by a number of considerations. First, to systematically study a number of rotational levels, it is necessary to excite the molecule with its own emission spectrum, since reliable tunable optical and uv sources with bandwidths $\lesssim 0.1$ Å are not yet available. In order to interpret the experiment, the spectrum must be reasonably well cataloged, so that identification of the states involved is unambiguous. Fortunately, the uv bands in OH have been thoroughly studied by a number of workers, most notably Dieke and Crosswhite.[7] Also, a reasonably intense OH emission spectrum is easily produced by rf discharge in water vapor.

Moreover, in common with other hydrides, OH has an untypically coarse rotational level structure because of its low reduced mass, resulting in a spectrum having some rotational lines isolated by as much as 1 Å from neighboring lines. These lines can be resolved by a relatively fast (low-resolution high-aperture) spectrometer so that the detection of resonantly scattered light may be limited to that from a single rotational level.

Finally, the OH radical is one of several diatomic molecules which are of astrophysical interest. A precise measurement of oscillator strengths is of considerable desirability for abundance determinations and for the understanding of other physical problems, and a large spread of values has existed in the literature.[8] The paper by Bennet and Dalby[8] contains a bibliography of other earlier work.

To date, direct measurement of the hyperfine splitting in the $A^2\Sigma$ state has eluded us: The size of the hfs interaction may be of some interest in elucidating the mechanism which leads to population inversion and subsequent maser-type emission in interstellar OH. Our current ODR measurements only serve to place a crude lower limit on the size of the splitting.

II. THEORY

We shall not review the existing literature on the theory of the Hanle effect as applied to atoms[1] and molecules[4]; we shall only mention certain features rarely arising in the more familiar atomic work, which greatly alter the experimental circumstances in the molecular Hanle effect.

We assume a geometry in which the direction of the incoming resonance light, direction of scattered radiation, and axis of the applied magnetic field are mutually orthogonal. Under these conditions, the usual theoretical description leads to an expression for the resonantly scattered light intensity given by

$$I = I_0 \pm I_s[1 + (2g_{J'}\tau\mu_B H)^2]^{-1}, \quad (1)$$

where I_0 represents a field-independent background scattering and I_s is the signal amplitude. The sign chosen for the signal term and the magnitude of I_s depends on the angular momentum quantum numbers J'', J', and J for initial, intermediate, and final states of the molecule.[8a] (In nearly all atomic work done to date, initial and final state J's are the same, and the minus sign is appropriate; the existence of both possible signs has not been explicitly displayed in most theoretical treatments of the Hanle effect.) In Eq. (1), $g_{J'}$ is the electronic g factor for the excited state of angular momentum J', τ is the mean life of the state, μ_B is the Bohr magneton, and H is the applied magnetic field strength. The signal width at half-maximum satisfies the equation $g_{J'}\tau = \hbar/2\mu_B H_{1/2}$ so that a measure of the field $H_{1/2}$ needed to reach half-signal amplitude yields a measure of the product $g_{J'}\tau$ for the excited state. The g factors may be separately determined by the ODR technique so that finally both g and τ are individually determined.

Zare[4] has published formulas for arbitrary J'', J', and J for a quantity which he calls the polarization. It can be shown that this is equivalent to I_s/I_0 in Eq. (1), which is the theoretical signal-to-background ratio. Convenient tabulations of this same quantity have also been given by Feofilov[9]; for the geometry chosen here, his Table 7 and Fig. 34 are the appropriate ones. Captions may be ignored; the numerical values give directly the signal-to-background ratios for various choices of $J'' \to J' \to J$.

The technique used in our experiments and described in detail in Sec. III involves fluorescent excitation of the sample by a broad band of resonance lines and selection of a single emission line ($J' \to J$) via a monochromator. Thus J' and J will be specified in principle by the monochromator setting, but J'' may have any of three values consistent with $\Delta J = 0, \pm 1$. Since one of these excitations may yield a Hanle signal with a sign opposite to the others, the resultant composite Hanle signal may be rather weak. The molecular Hanle signals are in any case usually weaker than in the atomic case, owing to the usually larger angular momentum of the states involved (see Ref. 9, Fig. 34). In OH and OD, our strongest Hanle signals were on the order of 3% of the field-independent background.

Thus far we have assumed a fairly simple situation for the structure of the angular momentum states; in practice ρ- or Λ-type doubling may be present along with hyperfine structure. Each J considered above is then replaced by individual values for the angular momentum of each of the sub-

levels within one of the resultant multiplets. A large number of routes over angular momentum values thus exist, consistent with the dipole-selection rules, each of which contributes a Hanle signal of differing amplitude and sign. In this more realistic case the resulting composite Hanle signal may be small indeed. Zare's or Feofilov's formulas may still be used, but the quantum numbers must be those of the total angular momentum including nuclear spin, and a summation must be made over all possible routes encompassed by the experimental resolution of the monochromator. This point will be given some further discussion in Sec. IV.

The $A^2\Sigma - X^2\Pi$ rotational band structure has been thoroughly cataloged by Dieke and Crosswhite.[7] On theoretical grounds, the $^2\Sigma$ state is expected to exhibit pure Hund's case b coupling (ignoring hfs effects), which is borne out by ODR measurements described here and by German and Zare.[5] The $^2\Pi$ ground state is described by coupling intermediate between cases a and b, with case b approached as J increases. Since the electronic spin $S=\frac{1}{2}$, there are two fine-structure states designated $\Pi_{3/2}$ and $\Pi_{1/2}$, respectively. For OH and OD it is customary to use the notation of Hund's case b for both the Σ and Π states. (We shall follow the transition-labeling scheme employed by Dieke and Crosswhite in all discussions below.) In the format of case b coupling, it is convenient to characterize various rotational states by the quantum number K, designating the total angular momentum without the electron-spin contribution S. Then $J=K\pm S$ for our particular case with $S=\frac{1}{2}$.

Each Π rotational state is split into two states of the same J and opposite parity by the Λ-doubling interaction,[10,11] and each Σ rotational state is split into two states of different J and the same parity by the ρ-doubling interaction.[10,11] For low values of K, the ρ doubling is on the order of a few hundredths of an angstrom for OH and the Λ doubling is somewhat smaller. Figure 1 indicates this structure, along with the standard notation and predicted transition intensities for the array of allowed transitions connecting a $K=4$ excited rotational state.

Each Λ and ρ doublet is further split by the magnetic hyperfine interaction. The hfs in the ground state has been measured with microwave techniques[11,12] and is ~ 55 MHz for the lowest $\Pi_{3/2}$ state of OH. The hfs splitting of the $^2\Sigma$ states is not known experimentally, but it must be smaller than the ρ doubling since the latter can be resolved by direct optical spectroscopy, while the hyperfine splitting has not been observed. The ρ doubling is $\simeq 6.8\,(K+\frac{1}{2})$ GHz in OH. There is good reason to believe that the hfs will be considerably larger in the Σ state than in the Π state of the hydroxyl molecule.

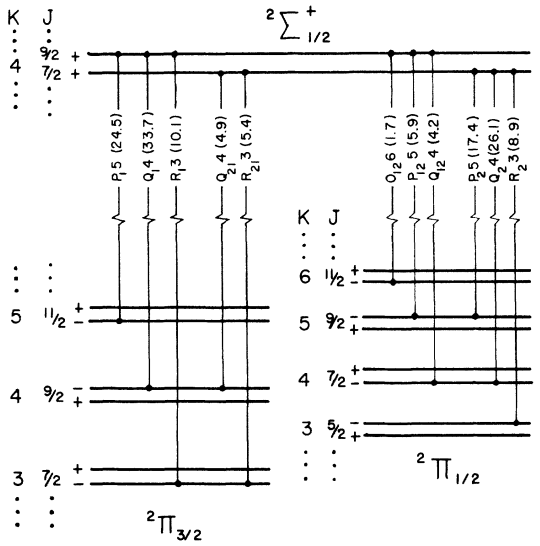

FIG. 1. Diagram of the transitions connecting the $K=4$ sublevel of the $A^2\Sigma$ state with the ground state for OH and OD. The hfs is not shown. The notation is that of Ref. 7.

We shall momentarily ignore the hfs and consider the theoretical g factors for the Σ state. Since the magnetic moment associated with K is very small compared to a Bohr magneton, the g factor is almost entirely determined by the magnetic moment of the electron spin. For case b coupling, the g factor for a state of angular momentum J is given by

$$g_J = \frac{J(J+1)+S(S+1)-K(K+1)}{2J(J+1)}\, g_s, \tag{2}$$

where g_s is the electronic-spin g factor. For $S=\frac{1}{2}$ and $g_s=2$, appropriate for a single unpaired electron, this reduces to

$$g_{K\pm 1/2} = \pm 1/(K+\tfrac{1}{2}). \tag{3}$$

The hfs modifies the g factors. For a given J state and nuclear spin I, the g factors of the hyperfine components F will be given by[13]

$$g_F = g_J \frac{F(F+1)+J(J+1)-I(I+1)}{2F(F+1)}, \tag{4}$$

where $I=\frac{1}{2}$ for OH and 1 for OD. Thus for a given ρ-doubled K state there are four or six hyperfine levels with somewhat different g factors. Since our apparatus cannot resolve either the ρ doubling or the hfs, each observed Hanle signal contains contributions from a number of hyperfine levels (all however from the same K value).

Note that although a main line and its ρ-doubled satellite (Fig. 1) come from sublevels of different J, Eqs. (2) and (3) show that the magnitude of g_J is the same in both cases, since both have the same K value.

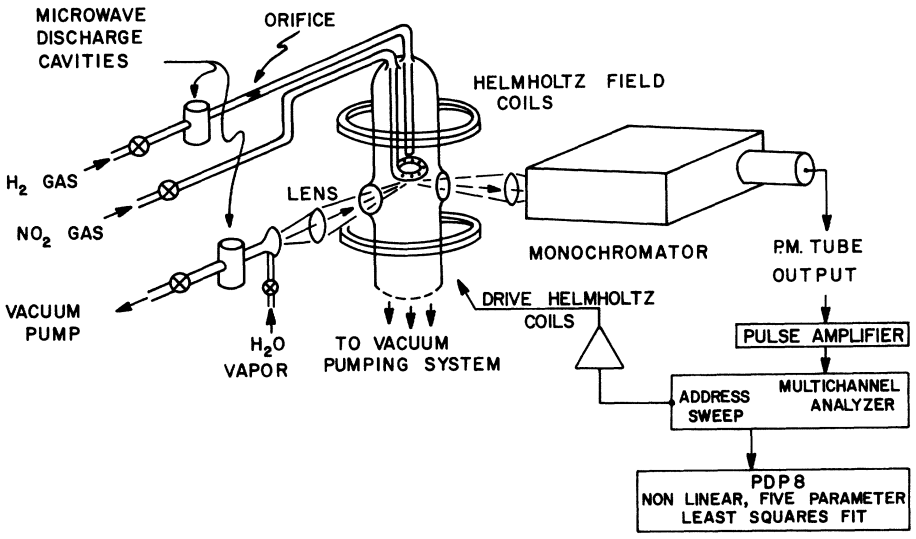

FIG. 2. Schematic diagram of the apparatus. The large auxilliary coils, the square Helmholtz coils, the rf antenna, and the mirrors are not shown.

III. EXPERIMENTAL APPARATUS

A sketch of the apparatus is shown in Fig. 2. OH resonance radiation from a 2450-MHz discharge in $\simeq 0.3$-Torr water vapor illuminates a sample of OH through a suitable optical system. The sample is produced by reacting atomic hydrogen with NO_2. Resonantly scattered light is focused onto the entrance slit of a monochromator adjusted to pass one of the wavelengths of interest, and is detected by a cooled photomultiplier at the exit slit. The detected photons are counted by a multiscalar used to average the signal. The OH sample is in a magnetic field produced by two sets of calibrated Helmholtz coils, one of which produces a temporal field ramp for sweeping through the signal. The apparatus is described in detail below.

A. Lamp

Light for resonance excitation of the molecules was produced by a 2450-MHz discharge in water vapor continuously pumped through a quartz lamp contained in an Evenson[14] cavity. The lamp was made from 12-mm tubing flared at the front end to a 25-mm-diam window. We have found that self-reversal is of little importance in the OH molecular lamp spectrum because the oscillator strength of each transition in each band is quite small.

The pressure in the lamp was controlled by a needle valve which admitted water vapor (or D_2O) from a reservoir at room temperature and was monitored by an air-calibrated thermocouple gauge. Typical readings were in the range 300–500 mTorr. With a nominal input of about 65 W to the lamp cavity, the output spectrum in the 3000-A region consisted primarily of the $A^2\Sigma$ 0-0 band. Since every feature in the observable spectrum of the lamp could be identified as a known OH transition, we conclude that there were no impurities of importance in the lamp spectrum.

B. Production of OH Molecules

OH and OD molecules were produced by reaction of atomic hydrogen (or deuterium) with NO_2 gas. Atomic hydrogen was produced in another 2450-MHz discharge in H_2 (or D_2), after bubbling the gas through H_2O (or D_2O), and flowed through about $\frac{1}{2}$ m of 12-mm quartz tubing before entering the reaction region. A narrow orifice in the flow tube just past the microwave discharge served to maintain sufficient pressure (a few millimeters of Hg) for a stable discharge, while allowing a much lower pressure (typically ≤ 1 μ) in the scattering region. Passage through this orifice did not seem to diminish substantially the number of free hydrogen atoms. NO_2 was controlled by a stainless-steel needle valve and was admitted to the reaction region through a glass "shower head" directed against the flow of H atoms immediately upstream from the optical-scattering region. The formation reaction is $H + NO_2 \rightarrow OH + NO$, and the dominant destruction reaction is $2OH \rightarrow H_2O + O$. Since the rate constant for decay is about 20 times smaller than the rate constant for formation, [15] we could obtain a sizable transient population of OH molecules. There was considerable variation of the efficiency of production with pressure, discharge conditions, and flow rates. We typically adjusted these parameters to achieve a stable production rate before each set of runs; once adjusted, fluctuations were quite small over periods of hours.

In this method of production only the $v = 0$ vibrational state seems to be produced with any appreciable population, and the rotational temperature very rapidly equilibrates at about room temperature. The latter was verified by a simple optical

bridge arranged to monitor the amount of resonance absorption when NO_2 was admitted to the reaction region in the presence of atomic hydrogen. Measurements were made as a function of the rotational quantum number J by a monochromator included in the optical bridge. If we let $\Delta I(J)$ equal the diminution in transmitted intensity $I(J)$ for the Jth rotational level when NO_2 is admitted, then plotting $\ln[\Delta I(J)/(2J+1)I(J)]$ vs

$$E(J) = \text{const} \times \{(J+\tfrac{1}{2})^2 - 1 \pm [2(J+1)+\lambda(\lambda-4)]^{1/2}\}$$

should result in a straight line with slope inversely proportional to the temperature if a Boltzmann distribution is assumed. Here λ is the ratio of the fine-structure coupling constant A to the rotational constant B for the ground $^2\Pi$ state, and $E(J)$ is the energy of the Jth rotational sublevel.[7,10] The data gave a good fit to a straight line indicating a temperature $T = 320 \pm 20\,^\circ\text{K}$. This is consistent with the result reported in Ref. 16, and effectively limited us to observations involving states for which $J \lesssim 8$ or 9 if usable Hanle signals were to be obtained within reasonable observing times.

The observed absorption was usually about 3% through the full width of the reaction cell (~ 10 cm). Since the observing region for 90° scattering in the Hanle and ODR experiments was confined to less than an 8-cm^3 central volume, the resonance lamp beam could properly be treated as illuminating the entire scattering region with undiminished intensity. It is also clear that radiation-trapping effects could be safely ignored.

C. Optical Arrangement

A pair of separated 50-mm-diam $f/2$ planoconvex quartz lenses collected and focused light from the lamp into the interaction region through a 50-mm-diam quartz window. A similar pair of lenses focused the fluorescent light onto the monochromator slits. The axes of the incident and fluorescent optical systems were perpendicular as shown in a top view of the optical system in Fig. 3. Two front-surface mirrors, made by aluminizing ordinary spherical watch glasses, were used to increase the amount of detected light. Each of them added about 50% to the count rate. In the ODR experiments the incident light was linearly polarized parallel to the field, but in the Hanle experiments, no polarizer was used.

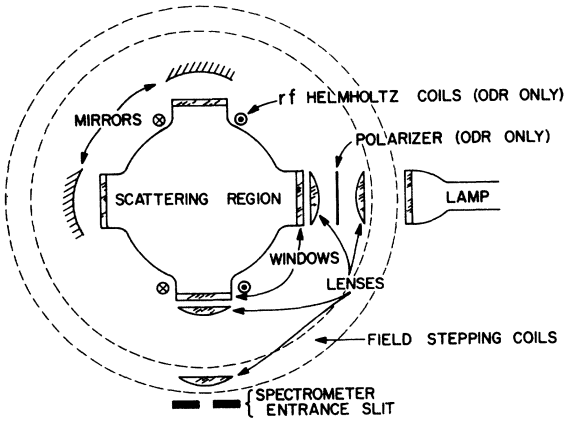

FIG. 3. Top view of the optical system showing more detail of the location of components. The lamp and monochromator are actually further out than the slightly distorted scale of the drawing indicates.

D. Scattered Light Detection

Because most of the strong components of the $A^2\Sigma$ 0-0 band were excited in the sample, a McPherson half-meter monochromator was employed to isolate specific rotational transitions for investigation. The monochromator had a dispersion of 13.3 Å/mm and was typically used with slit widths between 40 and 80 μ for the Hanle data, and 120 μ for the ODR experiments. An EMI 9526A tube with an S-13 cathode, cooled by dry ice, was used for the detector. Each photon pulse to the anode was current amplified by a transistorized amplifier mounted directly on the base of the tube. The amplifier rise and fall times were $\cong$ 0.5 μsec. The output of this amplifier went to an Ortec 410 amplifier for pulse shaping, and the bipolar output of the Ortec was fed to a Hewlett Packard 5245L counter which was used to monitor the counting rate. The unipolar output of the Ortec amplifier was fed to the input of a multichannel analyzer which was used as a signal averager.

E. Signal Averaging

Signal averaging was performed by a TMC model 404 multichannel analyzer used in its multiscaling mode. The analyzer was arranged so that it automatically made repetitive scans when in the "multiscaler" mode. We usually operated with a dwell time of 100 msec per channel and used only 100 channels of the memory. A typical 60-min run therefore consisted of about 360 sweeps, and the typical photon counting rate was ~ 4×10^3/sec. During an average Hanle run, we accumulate about 14 million counts distributed over 100 channels ($\simeq$ 140 000 per channel). The observed signal-to-noise ratio was about 10–12 for these runs, which is consistent with purely random noise sources, under our operating conditions in which the Hanle signal amounted to ~ 3% of the total scattered light. The weaker ODR signals required runs of 2–$2\frac{1}{2}$ h.

F. Magnetic Fields

The magnetic field was typically swept over several gauss. The sweeping field was produced by 23-cm-diam Helmholtz coils which were calibrated

[6.21(± 0.02) G/A] by a rubidium magnetometer of our own manufacture. The field current was typically determined to better than 3%, with the uncertainty due almost entirely to technical problems associated with end-transient measurements during the 10-sec stepped field sweep. The sweep was also determined to be linear to better than 1%.

The sweep was generated from the analog address of the TMC analyzer. The address signal was voltage amplified by a Hewlett Packard 2460A, current amplified by a Harrison Laboratories 6433B power supply, and then applied to the coils. During an experimental run, the voltage across a resistor in series with the coils was monitored on a strip chart recorder so that any drifts or irregularities of the sweep could be observed. Typically, none were found.

The sweep coils were enclosed in a set of 21-cm-square Helmholtz coils which reduced the horizontal component of the earth's field to less than $\frac{1}{2}$ mG in the experimental region. The vertical component of the earth's field was simply allowed to add to the vertical field produced by the sweeping and fixed coils.

For ODR experiments at fields higher than a few gauss, an auxilliary set of large heavy foil-wound Helmholtz coils was used to furnish a fixed biasing field. These coils were powered by a Magnion HS 1050 power supply that was stable to a few parts in 10^5. The coils were calibrated to an accuracy of $\simeq 0.3\%$ against the sweep coils, which had been previously calibrated by Rb optical pumping. The inhomogeneity over a 2.5-cm cube at the optical scattering region was less than 1:500.

G. rf Magnetic Field

For the ODR experiments, Zeeman transitions were excited by a set of coils in approximately the Helmholtz configuration, 8 cm diam, and consisting of 2 or 3 turns of BS 14 copper wire. They were oriented so that the rf magnetic field was parallel to the observation direction and perpendicular to the axis of quantization defined by the fixed and sweep fields (see Fig. 3). The oscillating rf field, decomposed into the standard counter-rotating circularly polarized components, induced $\Delta m = \pm 1$ transitions. The rf signal from a General Radio 1211C unit oscillator was amplified by a Heathkit DX60A transmitter and fed to the coils. The frequency was measured with a Hewlett Packard 5245L counter, and remained stable to better than $1:10^6$ during a run. Variable capacitors in series with the coils were used to make the antenna structure resonant at the desired frequency, resulting in high rf currents – typically 10 – 15 A. High power was necessary to obtain a measureable ODR signal, owing to the small population differences between neighboring Zeeman levels. Our signals were hence somewhat power broadened, but their centers could be measured with sufficient accuracy for our purposes. It was necessary to employ a shield designed to keep the electric field of the rf out of the interaction region in order to avoid electrical breakdown and discharge of the gases.

IV. DATA ACQUISITION AND PROCESSING

When the signal accumulated in the analyzer reached sufficient quality it was transmitted to a PDP 8/L computer for analysis, recorded with an X-Y recorder, and punched into paper tape for storage. The analysis consisted of a preliminary scan of the data for homogeneity followed by a rigorous least-squares fit.

The least-squares-fit program calculated a theoretical line shape $S(H)$ of some prespecified type (Gaussian, Lorentzian, etc.) which was further characterized by a number of adjustable parameters $V(I)$ (amplitude, width, dispersive component, etc.) and fitted to the experimental signal. The fitting process centers around an unweighted, nonlinear least-squares routine.[17]

For the present experiments, the theoretical line shape assumed for the fitting routine was Lorentzian. In many Hanle-effect runs, a sloping baseline was present ($\sim 1\%$ of the scattered amplitude over a 5-G scan) which was traceable to the influence of the fringing sweep field upon the lamp. Hence a sloping baseline was included as one of the variable parameters in the fitting routine. The presence of a dispersion component was also tested for; in either case, the effect of a sloping baseline or small dispersion component had only a slight effect ($< 1\%$) on the half-width at half-maximum.

The data from the ODR experiments were fitted with a Lorentizan doublet. The doublet arises from the two hyperfine components of an optical transition (see Fig. 4). The two lines were taken to have

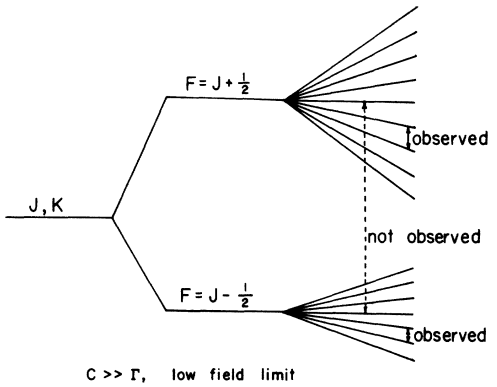

FIG. 4. Energy level diagram for $K' = 4$, $J' = \frac{7}{2}$, $F' = 4, 5$ levels in OH. The observed transitions in ODR are marked on the Zeeman part of the diagram. The same diagram applies to all rotational states except for the multiplicity of Zeeman sublevels.

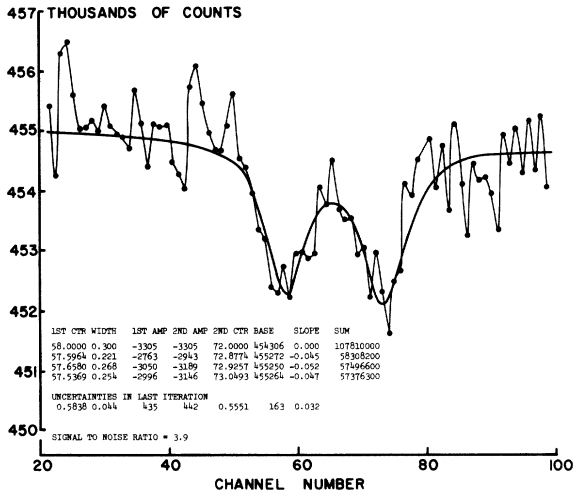

FIG. 5. Computer-fitted Lorentzian doublet (solid line) drawn through data points (connected dots) for a typical ODR run. The vertical scale shows that the signal is only about 0.7% of the background. The numerical inset is a copy of the computer output from the fitting procedure. Each line represents the results of an iteration. The sum of the residuals (at the right) is seen to decrease as the seven parameters approach their final values.

the same widths, but their amplitudes and spacing were among the floating parameters varied by the program. Figure 5 shows the computer output, the fitted line shape, and the data from a single typical ODR run. In cases where a sloping baseline appeared to be present, the data were fitted via a seven-parameter nonlinear fit; the parameters were two centers, two amplitudes, one width, baseline, and baseline slope. After a fit of a theoretical line shape to a set of data has been completed, the program uses the diagonal elements of the variance matrix from the last iteration to calculate the uncertainty associated with each of the parameters. These were used with the usual statistical procedures to assure us that there were no major artifacts in this fitting procedure.

V. RESULTS OF ODR EXPERIMENTS

A. g Factors

We have observed ODR signals from the first five rotational levels of the $A^2\Sigma$ state of OH. All observations were made on the Q-branch transitions ($\Delta K = 0$). The signal is observed when the sweeping magnetic field satisfies the condition $h\nu = \mu_B g H$, where the g factor of the excited Σ state is determined by the coupling of the three angular momenta S, I, and K. If there were no nuclear spin, the coupling would be pure Hund's case b since there is no orbital angular momentum (Σ state) and the g factor would simply be $g_J = 1/(K+\frac{1}{2})$. We now assume that the hfs is much larger than the Zeeman energy (weak-field limit) so that the g factor for the excited state $|KJF\rangle$ is instead given by Eq. (4). (This assumption is experimentally justified later.)

In our experiment we can determine K and J of the excited states by setting the spectrometer to select a particular emission line, but we cannot select F this way because the hfs splitting is very small. Since the experimental procedure was to fix an rf frequency and then sweep the external magnetic field, our ODR data showed two resonances. These occurred at the two field values corresponding to $F = J \pm I$. The observed rf transitions have been shown in Fig. 4, and a typical signal and fit have been shown in Fig. 5. The resonance condition $H = h\nu/\mu_B g$ was used to calculate g_{expt} from the magnetic field at the center of each ODR signal and values of g were averaged for each $|KJF\rangle$ state. The results are given in Table I along with the values expected from the relations above. All the experimental values of g are smaller than the values of g_{KJF}, but within experimental error. The data are plotted in Fig. 6.

The uncertainties in the experimental g factors in Table I are dominated by allowances for experimental systematic errors. The statistical uncertainties are less than 1.5% in all cases and less than 1% in most cases. There are several sources of possible systematic error; the largest is the uncertainty in the static measurements of the sweep amplitude which we conservatively estimate at 3%. Other sources of systematic error include calibration of the coils (0.3%), coil current measurements (2%), effect of rf pickup on reference circuits (1%), and several others, all less than 1%. We combine these and the statistical error and declare a total uncertainty of 5% on all the measurements in Table I.

We now return to the assumption that the Zeeman energy is much smaller than the hfs. The energy of the levels in Fig. 4 is given by the well-known Breit-Rabi equation

$$E = -\tfrac{1}{4}C + \Gamma m \pm \tfrac{1}{2}[C^2(J+\tfrac{1}{2})^2 + 2Cm(\Gamma_I - \Gamma) + (\Gamma - \Gamma_I)^2]^{1/2}, \quad (5a)$$

TABLE I. Comparison between experimental g factors and the value expected on the basis of case b coupling. The uncertainty associated with all experimental numbers is about 5% (see text).

K, J	$2, \frac{5}{2}$		$3, \frac{7}{2}$		$4, \frac{9}{2}$		$5, \frac{11}{2}$	
F	2	3	3	4	4	5	5	6
g_{expt}	0.462	0.320	0.319	0.242	0.238	0.193	0.193	0.163
g_{KJF}	0.467	0.333	0.321	0.250	0.245	0.200	0.197	0.167
No. of runs	6		9		10		2	

$$C = \pm b/(2K+1) + c/(2K+1)(2K+1\pm 2)\,, \qquad (5b)$$

where $\Gamma = g_J \mu_B H$, $\Gamma_I = g_I \mu_N H$, C is the J-dependent hyperfine constant, b and c are constants of the molecule,[13] and H is the magnetic field. The plus and minus signs go with $F = J \pm 1$. We expand this for the two extreme cases $\Gamma \ll C$ and $\Gamma \gg C$ and find that

$$E(m) - E(m-1) = h\nu_{\mathrm{ODR}} = \Gamma, \qquad \Gamma \gg C$$
$$E(m) - E(m-1) = h\nu_{\mathrm{ODR}} = \Gamma(2J+1 \mp 1)/(2J+1), \qquad \Gamma \ll C \qquad (6)$$

if we neglect Γ_I. Notice that for small values of C there is only one ODR frequency but for large values of C there are two frequencies. We conclude that C is much larger than the Zeeman energies in this experiment since we observed two signals at two separate values of magnetic field for a given frequency.

B. Hyperfine Structure

It is clear that as the Zeeman energies of the observed ODR transitions get larger the effects of the higher-order terms in the expansion of Eq. (5) become important. If the next-higher-order term in the expansion for $\Gamma \ll C$ is retained and we calculate ν_{ODR} in terms of Γ and then solve for Γ, there are two solutions to the resultant quadratic equation, Γ_+ and Γ_-, corresponding to the two observed signals. We define the dimensionless parameter X by

$$X \equiv \frac{\Gamma_+ - \Gamma_-}{\Gamma_+ + \Gamma_-} = \frac{1}{2J+1} - \frac{2(2m-1)}{J^3}\,\frac{\nu_{\mathrm{ODR}}}{C} \qquad (7)$$

after some more algebra. The average value of $|2m-1|$ is $(4J^2-1)/4J$. We determine the frequency dependence of X using the values calculated from our measured ODR frequencies. The resulting experimental upper limit on $dX/d\nu_{\mathrm{ODR}}$ is used to set a lower limit on C and consequently on the hfs splitting. We find that the lower limits on the hfs are 240, 550, and 330 MHz from our data on $K' = 2, 3$, and 4, respectively. These numbers suggest a crude lower limit of about 700–900 MHz for the splitting of the $K = 1$ level of the $^2\Sigma_{3/2}$ state in OH. The limit in OD is expected to be reduced in direct proportion to the smaller nuclear moment.

It is obvious that better determinations of the hfs could be made if the range of our ODR measurements were extended to higher frequencies and fields. We were not successful in this because the signals became weaker and disappeared as we raised the frequency. We can only speculate on the reasons.

C. Other Results from ODR

We have compared the width of our ODR signals with the expected width calculated on the basis of the measured rf power and an approximate lifetime. We find that our signals do not display the expected power broadening; in fact, they are usually only slightly broader than the natural width. We conclude that the sample is somewhat shielded from the rf magnetic field, probably by the rf electric shield. This shielding becomes more effective at higher frequencies and is probably responsible for our loss of signal.

The m dependence of X indicates that the ODR signals should broaden and eventually split at higher frequency. Since we could not separate this effect from power broadening, it could not be used to provide a reliable lower limit for the hfs.

The amplitude of the ODR signals was usually between 0.5 and 1% of the total scattered light, which was typically 2000 photons/sec. It was usually necessary to accumulate data for 2 h in order to achieve a signal-to-noise ratio of about 4 in our 100-channel analyzer. Consequently, linewidth measurements are not accurate to better than about 25%. The relative amplitudes of the two ODR signals showed no consistent pattern, but the amplitude of the $F = J + I$ signal was larger more often than not.

VI. RESULTS OF HANLE-EFFECT EXPERIMENTS

A. hfs Considerations

We have observed the Hanle effect in four rotational levels of OH ($K = 2$–5) and in seven rotational levels of OD ($K = 2$–8). Most of the observations were in the Q-branch fluorescence because it is the strongest, but observations were also made in the P and R branches. The fluorescence was observed through the monochromator which could be used to determine K and J of both excited and ground states of the fluorescent transition. However, the excitation was achieved with a lamp emitting the entire OH spectrum so that any given excited state could be populated via the several upward transitions of the P, Q, and R branches and their satellites. Since the width of the Hanle signal (the only experimental parameter of interest here) depends only on the lifetime and g factor of the excited state, it appears that spectrometer selection of the excited state should provide a signal whose width is unambiguous. This is certainly the case for a molecule with hfs large enough to be separated by the monochromator or equal to zero, but neither of these conditions is met for OH and OD.

Each excited-state level determined by J' and K' may have two or three hyperfine sublevels with different g factors (see discussion in Sec. V A), and consequently the Hanle signal observed from a given hyperfine multiplet is composed of a sum of several signals of varying widths, amplitudes, and

signs, one from each unresolved hyperfine component. The following discussion shows that the width of this composite Hanle signal in OH and OD is almost the same as if there were no hfs.

We will assume that the width of the composite signal can be given by $H_{1/2}=\hbar/2\mu_B \tau g_{eff}$, where $g_{eff}=\sum IPg_{KJF}/\sum IP$ is a linearly weighted average of the g factors of all the transitions that contribute to the signal.[18] Here I is the intensity of a transition whose Hanle signal strength is P, and the sum is over all hyperfine sublevels of the excited and ground state which contribute to the signal. The strength of the Hanle signal $P\equiv I_s/I_0$ depends on the change of the angular momentum quantum number during excitation as well as during decay. We define a "route" as the sequence of initial, excited, and final states of a molecule when the transition from excited to final state produces a photon which contributes to the Hanle signal. The sums above are taken over initial states of three branches of excitation. If the hfs were zero, there would be three terms in the sums (neglecting satellite lines); for the case of OD with $I=1$, there are 45 terms in the sums.

The calculation of the values of I is straightforward. The intensity of a route is

$$I=\sum_{M''M'M}|\langle K''S''J''I''F''M''|T(k',q)|K'S'J'I'F'M'\rangle\langle K'S'J'I'F'M'|T(k,q)|KSJIFM\rangle|^2 \quad (8)$$

in the notation of Edmonds.[19] This can be reduced to

$$I=|\langle K''SJ''||T(k')||K'SJ'\rangle\langle K'SJ'||T(k)||KSJ\rangle|^2(2F+1)(2F''+1)(2F'+1)^2(6J_1)^2(6J_2)^2, \quad (9)$$

where the $6J$ symbols are given by[19]

$$(6J_1)=\begin{Bmatrix}J''F''I\\F'\ J'\ 1\end{Bmatrix} \quad \text{and} \quad (6J_2)=\begin{Bmatrix}J'F'I\\F\ J\ 1\end{Bmatrix}. \quad (10)$$

The first reduced matrix element in the equation above is constant for all routes selected by the spectrometer; the second depends only on the excitation branch.

Once the values of F'', F', and F for a route have been specified for the calculation of I, they are used to determine P as well. This could be done rigorously by using the Breit[20] formula, but we have chosen to use the summary given by Zare.[4] Formulas in his Table IV give the degree of polarization of resonantly scattered light for orthogonal geometry; this can be shown to be the same as the strength of the Hanle signal we observe, defined as the ratio of signal amplitude to total scattered background.

Some results of the calculation of g_{eff} are shown in Table II. We present some values of g_{eff} for OD for each of the three main excitation branches sep-

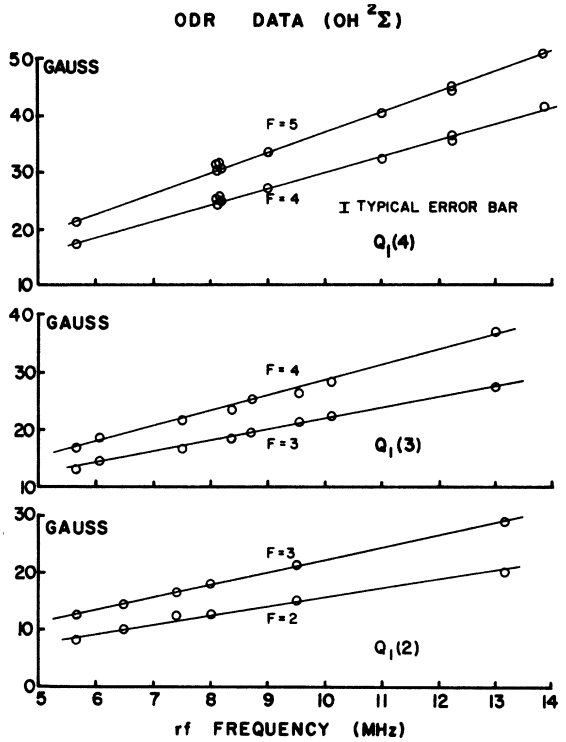

FIG. 6. Plot of the location of the centers of the ODR signals vs magnetic field. There are two sets of data for each transition arising from the two hfs components. A typical error flag is shown.

TABLE II. Values for g_{eff} for the OD molecule in its $A^2\Sigma$ state calculated by the procedure described in the text. The g_{eff} is given separately for each absorbtion branch. In order to get the final g_{eff}, the entries in a particular column should be weighted by the second $6J$ symbol in Eqs. (9) and (10) and summed. The sum should be divided by the sum of the $6J$ symbols used in the weighting. The results of this procedure are essentially identical to $1/(K'+\frac{1}{2})$ which ignores hfs effects. [There are only 14, 14, and 10 terms, respectively, in the sums on the $P1(5)$ emission.]

Absorption branch	Emission branch, K' $Q1(2),2$	$Q1(4),4$	$P1(5),4$	$Q1(8),8$	No. of terms in sum
P	0.3878	0.2219	0.2229	0.1181	14
Q	0.4034	0.2226	0.2217	0.1174	17
R	0.4099	0.2231	0.2230	0.1178	14
$1/(K'+\frac{1}{2})$	0.4000	0.2222	0.2222	0.1177	

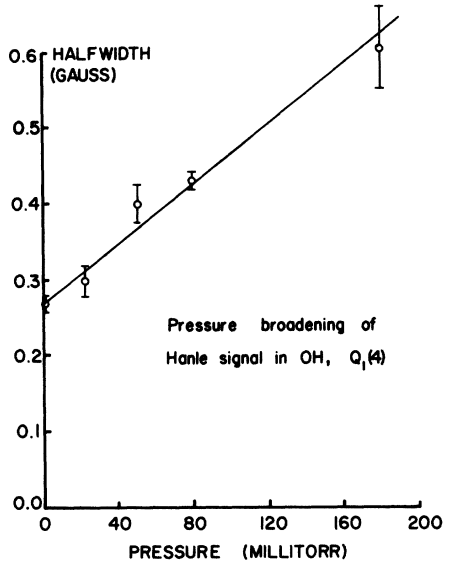

FIG. 7. Pressure broadening of the OH Hanle-effect signal. Only the total pressure in the cell is plotted.

arately. Each value of g_{eff} therefore represents contributions from three values of F'', F', and F for given values of K'', K', K, J'', J', and J. (Some contributions vanish because of the transition selection rules.) We emphasize that K', K, J', and J are determined by the setting of the spectrometer for any experimental observation. The results for OH show similar agreement. We conclude that we can neglect the effects of the hfs for the purpose of interpreting our Hanle-effect data. Throughout this calculation we have assumed that the exciting light is "white" over the hyperfine splitting. This is probably a safe assumption, since the hfs has never been detected optically, implying that it is less than the typical lamp Doppler width of ~2.5 GHz.

TABLE III. Results from the present Hanle-effect measurements on OH and OD compared with other published values for the lifetime of the $A^2\Sigma$ state. The total uncertainty in the present work is the combination of the statistical uncertainty σ_{stat} and the 3% experimental uncertainty. The lifetimes for all K values have been averaged together in the present work.

Species	Lifetime of the $A^2\Sigma$ state (nsec)	Remarks
OH	660(22)	Present work, 48 runs, $\sigma_{stat}=10$ nsec
OH	777(39)	Hanle effect with atomic overlap[a]
OH	850(130)	Phase-shift technique[b]
OH	1010(50)	Excitation decay[c]
OH	442(40)	Hook method[d]
OD	598(20)	Present work, 31 runs, $\sigma_{stat}=9$ nsec
OD	630(70)	Hanle effect with atomic overlap[e]
OD	850(100)	Phase-shift technique[b]

[a] Reference 5.
[b] W. H. Smith (private communication).
[c] Bennet and Dalby, Ref. 8.
[d] Anketell and Pery-Thorne, Ref. 8.
[e] German and Zare, Ref. 8.

B. Pressure Broadening

We have varied the pressure of the gases in the scattering region in order to determine the effects of pressure broadening on our measurements. The results are shown in Fig. 7. Note that the graph of the same data published in Ref. 3 is misleading because the vertical axis is improperly labeled. We have always taken Hanle and ODR data at pressures below 1 mTorr in order to avoid errors from pressure broadening. At 1 mTorr the signal is pressure broadened by about 0.6%.

C. Experimental Results

The half-width at half-maximum of a Hanle signal is given by $H_{1/2}=\hbar/2\mu_B g\tau$. Our ODR measurements indicate the g factors of the excited states can be calculated from pure Hund's case b coupling, and our calculations indicate that the width of the

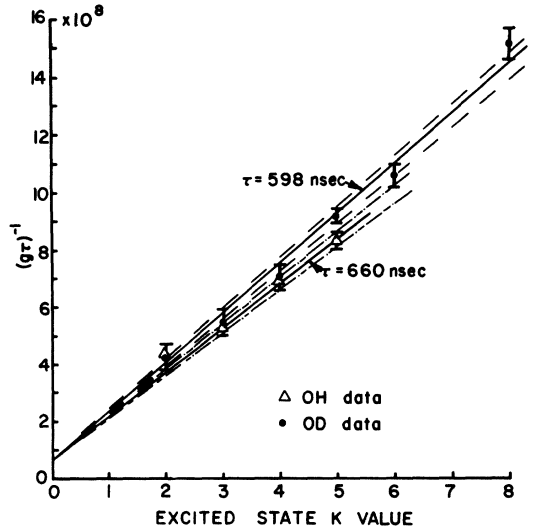

FIG. 8. Values of $(g\tau)^{-1}$ calculated from the widths of the Hanle-effect signals are plotted against K of the $A^2\Sigma$ state. The broken lines represent 3% deviation from the solid lines.

Hanle signal may be treated as if the signal arose from a single rotational level and not a hyperfine multiplet. Our measurements of $H_{1/2} \propto 1/g\tau$ therefore yield a direct measurement of the lifetime of the excited states.

If $g = 1/(K' + \frac{1}{2})$ is substituted into the expression for $H_{1/2}$ the result is

$$H_{1/2} = (K' + \tfrac{1}{2})\hbar/2\mu_B\tau . \quad (11)$$

We have used Eq. (11) to calculate τ from each Hanle-effect run and then averaged the values of τ obtained from all runs. The value of K' was determined by the spectrometer setting. We have found that the measured lifetimes of all rotational states are equal within experimental error. The results are summarized in Table III and compared with the results of other workers. The statistical uncertainty in Table III is the usual standard deviation divided by the square root of the number of runs. The total experimental uncertainty is 3% and comes from the previously mentioned difficulty with the field sweep calibration. Since we do not measure the position of the center of the Hanle signal, none of the other sources of systematic error discussed for ODR affect our results.

In Fig. 8 the measured values of $H_{1/2}$ for OH and OD are plotted against K'. The slope and intercept of the solid lines are given by Eq. (11) with our experimental values of τ; the dashed lines represent 3% variations.

Table III and Fig. 8 indicate that the lifetime for OH and OD are different by almost 1.5 times the total uncertainty. We do not know of any theoretical reason why this should be so, and believe the discrepancy should be regarded as a statistical fluctuation. We recommend the mean, 629 ± 22 nsec, for the lifetime of the $^2\Sigma$ state.

ACKNOWLEDGMENT

We wish to acknowledge the help of Michael Wiest in taking much of the ODR data.

*Present address: c/o Sawyer, RFD 2, Garrison Lane, Scarborough, Me.

[1]R. L. de Zafra and W. Kirk, Am. J. Phys. 35, 573 (1967); A. Lurio, R. L. de Zafra, and R. J. Goshen, Phys. Rev. 134, A1198 (1964).

[2]D. R. Crosley and R. N. Zare, Phys. Rev. Letters 18, 942 (1967) [unfortunately, these first-reported molecular-level-crossing results were later discovered to be due to mercury contamination and are being repeated – R. N. Zare (private communication)]; S. J. Silvers, T. H. Bergeman, and W. Klemperer, J. Chem. Phys. 52, 4385 (1970).

[3]A. Marshall, R. L. de Zafra, and H. Metcalf, Phys. Rev. Letters 22, 445 (1969).

[4]R. N. Zare, J. Chem. Phys. 45, 4510 (1966).

[5]K. R. German and R. N. Zare, Phys. Rev. Letters 23, 1207 (1969); Phys. Rev. 186, 9 (1969).

[6]W. C. Wells and R. C. Isler, Phys. Rev. Letters 24, 705 (1970).

[7]G. H. Dieke and H. M. Crosswhite, J. Quant. Spectry. Radiative Transfer 2, 97 (1962).

[8]K. R. German and R. N. Zare, Bull. Am. Phys. Soc. 15, 82 (1970); W. H. Smith (private communication); R. G. Bennet and F. W. Dalby, J. Chem. Phys. 40, 1414 (1964); J. Anketell and A. Pery-Thorne, Proc. Roy. Soc. (London) A301, 343 (1967).

[8a]*Footnote added in proof.* We shall generally adhere to the convention of using primes in this manner to designate quantum numbers for specific states. In some portions of the text primes have been omitted where ambiguity is minimal.

[9]P. P. Feofilov, *The Physical Basis of Polarized Emission* (Consultants Bureau, New York, 1961).

[10]G. Herzberg, *Molecular Spectra and Molecular Structure: I. Spectra of Diatomic Molecules* (Van Nostrand, Princeton, N. J., 1957).

[11]G. C. Dousmanis, T. M. Sanders, and C. H. Townes, Phys. Rev. 100, 1735 (1955).

[12]H. E. Radford, Phys. Rev. 126, 1035 (1962); Phys. Rev. Letters 13, 534 (1964).

[13]R. A. Frosch and H. M. Foley, Phys. Rev. 88, 1337 (1952).

[14]F. C. Fehsenfeld, K. M. Evenson, and H. P. Broida, Rev. Sci. Instr. 36, 294 (1965).

[15]F. P. del Greco and F. Kaufman, Discussions Faraday Soc. 33, 128 (1962).

[16]D. M. Golden, F. P. del Greco, and F. Kaufman, J. Chem. Phys. 39, 3034 (1963).

[17]The routine has been programmed from the recipe given by Wentworth, J. Chem. Educ. 42, 96 (1965).

[18]Of course, the signal is *not* a single Lorentzian whose width is determined by a linearly averaged g_{eff}, but a sum of several different Lorentzians. The least-squares-fitting procedure may not choose exactly the half-width in order to get the best fit; it might very well settle on some other effective width. We have therefore done a series of calculations to determine the effect of the fitting procedure. In particular, we have produced Lorentzian curves of varying amplitudes and widths, added them, and allowed our usual data-processing program to fit them. The results of the fit are then compared with a linearly averaged g_{eff} calculated from the input curves. For all sizes and widths of input signals with experimental range, the results indicate that a linearly averaged g_{eff} is a very accurate representation of the width of the signal. Even for the extreme case of only two contributions, differing in strength by a factor of 2 and in width by 25%, the fitted width was within 3% of the linearly averaged width.

[19]A. R. Edmonds, *Angular Momentum in Quantum Mechanics* (Princeton U. P., Princeton, N. J., 1957), see p. 75, Eq. 5.4.1, and p. 111, Eq. 7.1.7.

[20]G. Breit, Rev. Mod. Phys. 5, 91 (1933); V. Weisskopf, Ann. Phys. (N.Y.) 9, 23 (1931).